Supporting information

for

Strain-mediated interlayer coupling effects on the excitonic behaviors in an epitaxially-grown MoS$_2$/WS$_2$ van der Waals heterobilayer

Sangyeon Pak,[†] Juwon Lee,[†] Young-Woo Lee,[†] A-Rang Jang,[†, ‡] Seongjoon Ahn,[‡] Kyung Yeol Ma,[‡] Yuljae Cho,[†] John Hong,[†] Sanghyo Lee,[†] Hu Young Jeong,[§] Hyunsik Im,[∥] Hyeon Suk Shin,[‡] Stephen M. Morris,[†] SeungNam Cha,[†,]* Jung Inn Sohn,[†,]* and Jong Min Kim[⊥]

[†] Department of Engineering Science, University of Oxford, Parks Road, Oxford OX1 3PJ, United Kingdom

[‡] Department of Chemistry and Department of Energy Engineering, Low-dimensional Carbon Materials Center, Ulsan National Institute of Science and Technology (UNIST), UNIST-gil 50, Ulsan 44919, Republic of Korea

[§] UNIST Central Research Facilities (UCRF), Ulsan National Institute of Science and Technology (UNIST), 50 UNIST-gil, Ulsan 44919, Republic of Korea

[∥] Division of Physics and Semiconductor Science, Dongguk University, Seoul 100-715, Republic of Korea

[⊥] Department of Engineering, University of Cambridge, 9 JJ Thomson Avenue, Cambridge CB3 0FA, United Kingdom

* Corresponding author. Tel: +44-1865-273912. Fax: +44-1865-273010.

E-mail address: seungnam.cha@eng.ox.ac.uk, junginn.sohn@eng.ox.ac.uk

Experimental Section

<u>Material synthesis: Growth of the MoS$_2$/WS$_2$ heterostructure using CVD</u>

The epitaxial heterostructures were grown on a SiO$_2$ (300 nm)/Si substrate using a chemical vapour deposition (CVD) method. In summary, the synthesis was carried out inside a 2 inch tube furnace by placing a mixture of MoO$_3$/WO$_3$ precursors (typically 0.1 mg and 10 mg each, >99% Sigma Aldrich) on the alumina boat while another alumina boat containing S powders (200 mg, >99.98 % Sigma Aldrich) was placed upstream of the tube furnace. The SiO$_2$/Si substrate was placed on the boat containing MoO$_3$/WO$_3$ precursors with it facing down. The furnace was heated to 200 °C while flowing ultrahigh-pure argon at atmospheric pressure with 1000 sccm for 30 minutes to make the chamber a very clean argon environment. The procedure of growth is: ramp temperature at 18.75 °C/min up to 750 °C, continue at a temperature of 750 °C for 10 minutes with an Ar gas flow of 150 sccm, and the furnace was, then, naturally cooled down to room temperature. MoS$_2$ is grown first on the SiO$_2$ substrate and subsequent WS$_2$ was grown on top of the MoS$_2$.

<u>Wet transfer of the MoS$_2$-WS$_2$ heterostructure onto a PET substrate</u>

The as-grown MoS$_2$/WS$_2$ heterostructure on a SiO$_2$/Si Substrate was transferred onto a flexible PET substrate with 125 μm thickness via a standard wet transfer process. The as-grown samples were spin coated with PMMA (950 PMMA A8), and the substrate was baked on a hot plate at 120 °C for 5 minutes. Then, the substrate was floated on a KOH solution of 1M in order to wet etch the underlying SiO$_2$ substrate at 90 °C. The remaining PMMA coated MoS$_2$/WS$_2$ heterostructure sample was finally rinsed several times in DI water and transferred onto the 1 cm x 1 cm PET substrate and baked for further 5 minutes at 90 °C.

Characterizations of the TMDCs crystals

The PL and Raman measurements were performed on a Jobin Yvon LabRam Aramis confocal- Raman spectroscopy system using a 532 nm excitation source. PL spectra were acquired for a power of 20 µW and Raman spectra were acquired for an excitation power of 1 mW.

Density functional theory analysis of monolayer MoS$_2$ and WS$_2$ under strain

Local density approximation (LDA) was used to model the electronic band structures of monolayer MoS$_2$ and WS$_2$ according to the Ceperlay Alder (CA) parameterization. The lattice parameters were optimized and the atomic positions were relaxed until convergence tolerance of 1×10^{-2} eV/□ and the energy of 5×10^{-7} eV. The plane wave cut-off energy of 720 eV was used. A vacuum spacing larger than 20 □ was added to hinder the interaction between the periodic replicas along the c-direction. Strain was induced by adding external stress to the lattice. Strain applied was then calculated using $\varepsilon = \frac{a-a_0}{a_0} \times 100\%$, where a is the lattice parameter of the strained monolayer and a_0 is the optimized lattice constant
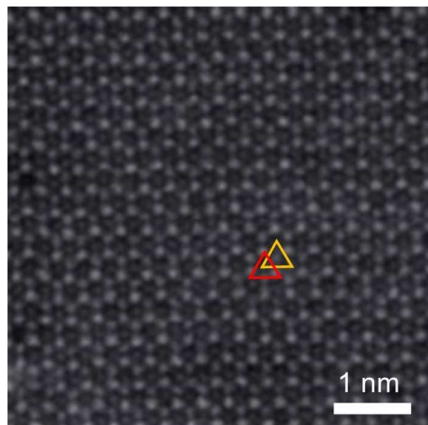
Figure S1. High angle annular dark field scanning transmission electron microscopy (HAADF-STEM) image of our MoS_2/WS_2 heterobilayer, showing that the heterobilayer has AA-stacking with the 3R phase.

The stacking order of CVD-grown TMDCs homobilayers and heterobilayers can be discerned through relative orientation angles between the bottom layer and the top layer.[1-4] Stacking angles of 0º (AA-stacking) and 60º (AB-Stacking) are most commonly observed in CVD-grown TMDC bilayers due to their energetically most stable configurations, and they correspond to the 3R and 2H phases, respectively, of TMDCs crystals. The HAADF-STEM image of our MoS_2/WS_2 heterobilayer clearly shows an atomic structural configuration with the 3R crystal phase. Moreover, it is also confirmed that our heterobilayer has 0º stacking orientation (AA-stacking) with the 3R phase as observed through the optical image and AFM image in Figure 1b and Figure 1c, respectively.
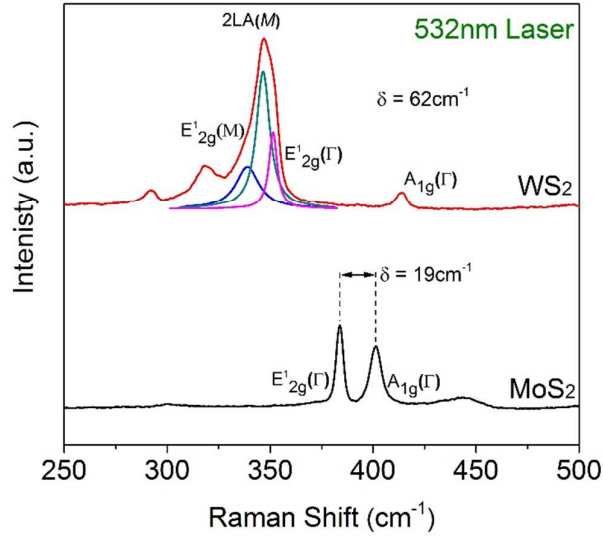
Figure S2. Raman spectrum of monolayers of MoS_2 and WS_2. The WS Raman vibrational modes were extracted using multi-Lorentzian fitting.

Under excitation with a 532 nm laser, the Raman spectrum of WS_2 reveals many second-order peaks such as the distinct 2LA mode at the M point, which are much stronger than the first order in-plane and out-of-plane modes. Therefore, multi-Lorentzian fitting was employed to show the presence of the distinct WS_2 Raman characteristic modes (E^1_{2g} and A_{1g}). The magnitude of the peak differences between E^1_{2g} and A_{1g} is one of the key parameters used for estimating the number of layers in a 2D TMDC. The peak difference of 62 cm^{-1} and 19 cm^{-1} for WS_2 and MoS_2, respectively, clearly confirms that the WS_2 and MoS_2 are monolayers.

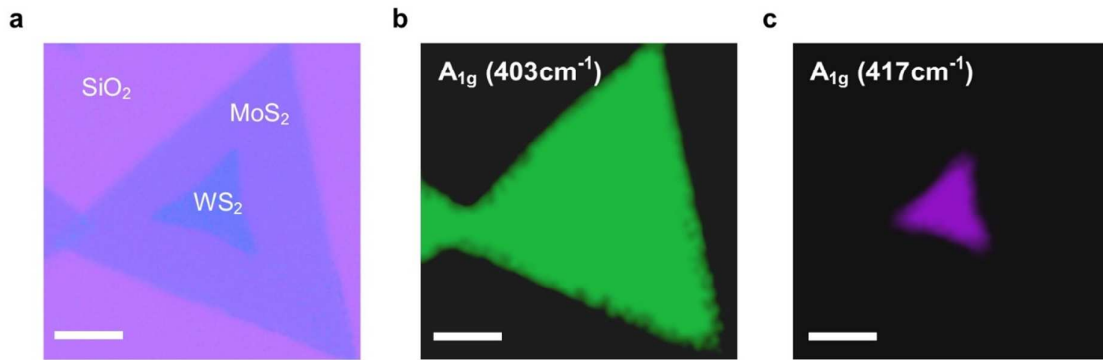**Figure S3.** (a) Optical image of a MoS_2/WS_2 heterobilayer. Raman intensity mapping images of (b) the MoS_2 A_{1g} mode peak (403 cm^{-1}) and (c) the WS_2 A_{1g} mode peak (417 cm^{-1}). These images demonstrate that the vertically stacked heterostucture consists of monolayers of MoS_2 and WS_2. Scale bars: 10 μm.
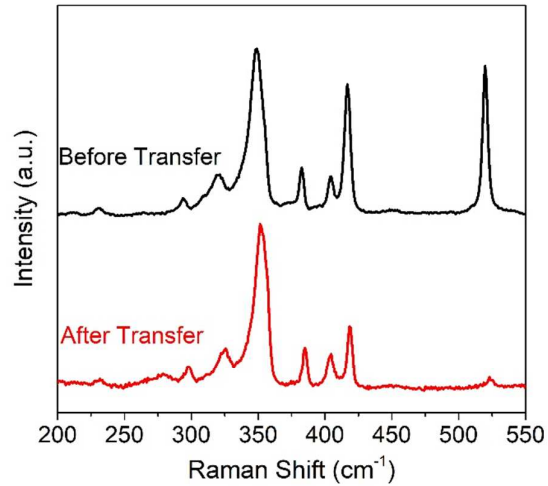
Figure S4. Raman spectra of the MoS_2/WS_2 heterobilayer before (on SiO_2) and after transfer (onto PET substrate).

After the transfer, a slight blue shift as well as slightly reduced intensity of the WS_2 A_{1g} phonon mode was observed. This might be because transferring of the sample can release the tensile strain that normally arises when fabricating on SiO_2, which is due to the mismatch in the thermal coefficients between the substrate and the deposited materials and this in turn results in a blue shift of both the MoS_2 and WS_2 Raman peaks.
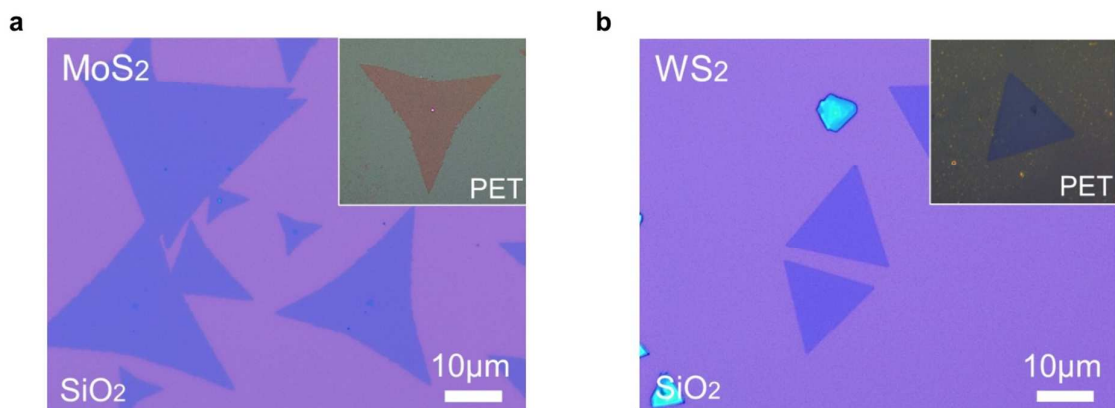
Figure S5. Optical image of the CVD-grown monolayer (a) MoS_2 and (b) WS_2 on SiO_2 with well-defined side facets and optical contrast. Blue and violet indicate MoS_2/WS_2 crystals and 300 nm SiO_2 substrate, respectively. Scale bars: 10 μm. The inset images show the monolayer MoS_2 and WS_2 atomic crystals, transferred to the PET substrate in order to investigate the strain-dependent properties.
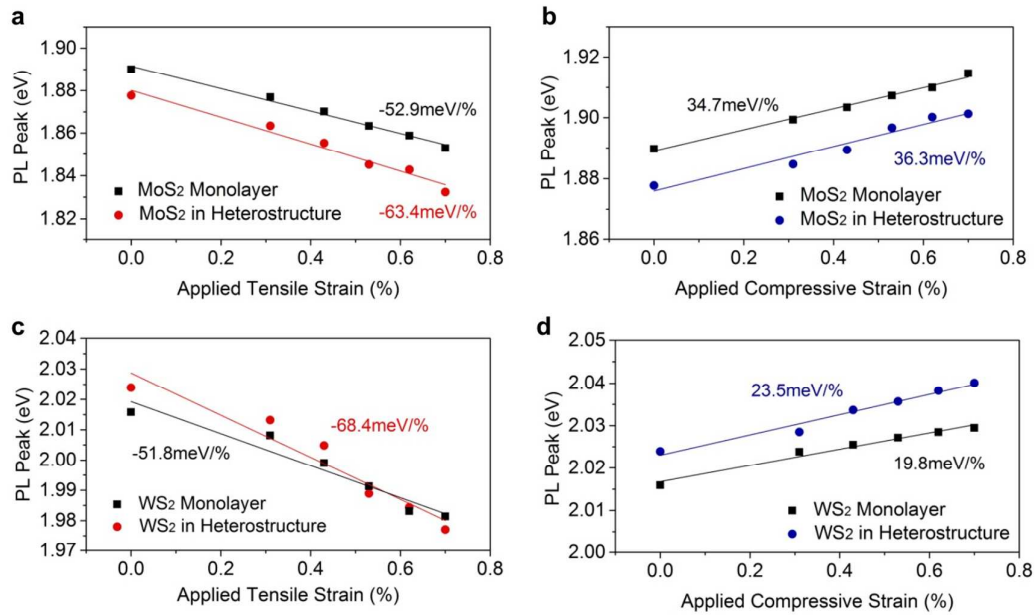
Figure S6. Strain-dependent PL peak shift in monolayers and heterobilayer under tensile and compressive strain for (a,b) MoS_2 and (c,d) WS_2.

The magnitude of the peak shift rates in the PL is a direct indication of a modulation of the electronic band structure. We have investigated the change in the PL spectra of individual monolayers of MoS_2 and WS_2 under tensile and compressive strains and compared this to the magnitude of the shifts with those of the MoS_2/WS_2 heterobilayer. A significant modulation of the PL peak was observed in each of the MoS_2 and WS_2 PL peak of the heterobilayer compared to the monolayer PL peaks under tensile strain, indicating the effect of the interlayer interaction.
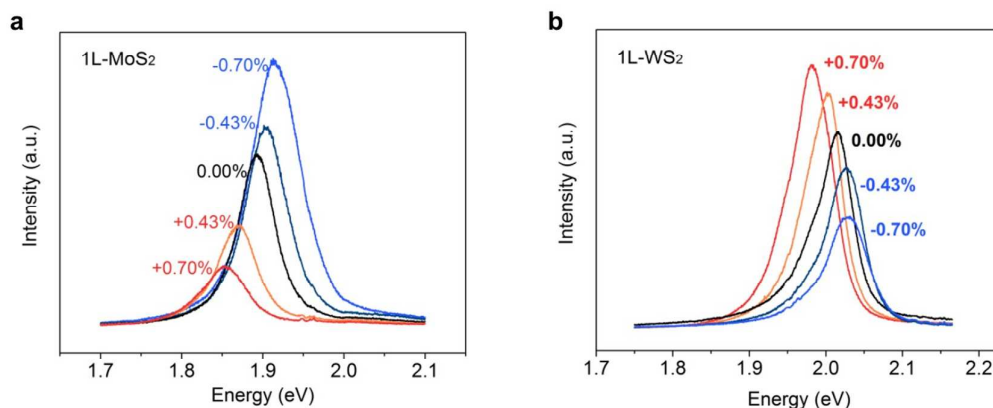
Figure S7. Strain-dependent PL spectra of monolayers of (a) MoS_2 and (b) WS_2 under tensile and compressive strains. The positive and negative signs indicate tensile and compressive strains, respectively. Under tensile strain, a monolayer of MoS_2 undergoes a direct-to-indirect transition of the band gap (PL intensity decreases) whereas WS_2 enhances the direct band gap characteristic (PL intensity increases). On the contrary, under compressive strain the direct band gap characteristics of the monolayer MoS_2 are enhanced while for the WS_2 monolayer, a direct-to-indirect transition is observed. These experimental observations directly support the opposing behaviours in the band structure for the monolayers of MoS_2 and WS_2 under tensile and compressive strain.
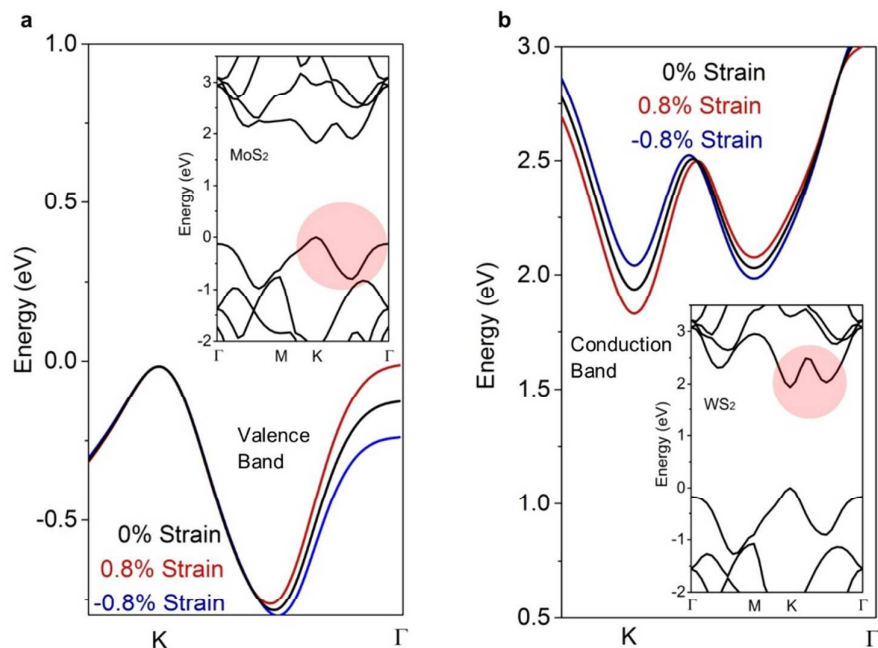
Figure S8. Density functional theory (DFT) calculations further confirm clear contrasting evolution of band structure in (a) MoS_2 and (b) WS_2. For MoS_2, the transition is governed by the change in the energy level of the local valence band maxima at the Γ-point, and for WS_2, the transition is governed by the opposite shift in the conduction band energies at the K and K-Γ points. The inset images show band structure of MoS_2 and WS_2 at zero strain.

Supporting Information References

(1) Xia, M.; Li, B.; Yin, K.; Capellini, G.; Niu, G.; Gong, Y.; Zhou, W.; Ajayan, P.; Xie, Y-H. *ACS Nano* **2015**, 9, (12), 12246-12254.

(2) Gong, Y.; Lie, S.; Ye, G.; Li, B.; He, Y.; Keyshar, K.; Zhang, X.; Wang, Q.; Lou, J.; Liu, Z.; Vajtai, R.; Zhou, W.; Ajayan, P. M. *Nano Lett.* **2015**, 15, 6135-5141.

(3) Zhang, J.; Wang, J.; Chen, P.; Sun, Y.; Wu, S.; Jia, Z.; Lu, X.; Yu, H.; Chen, W.; Zhu, J.; Xie, G.; Yang, R.; Shi, D.; Xu, X.; Xiang, J.; Liu, K.; Zhang, G. *Adv. Mater.* **2016**, 28, 1950-1956.

(4) Liu, K.; Zhang, L.; Cao, T.; Jin, C.; Qiu, D.; Zhou, Q.; Zettl, A.; Yang, P.; Louie, S. T.; Wang, F. *Nat. Commun.* **2014**, 5, 4966.

(5) Yan, J.; Xia, J.; Wang, X.; Liu, L.; Kuo, J-L.; Tay, B. K.; Chen, S.; Zhou, W.; Liu, Z.; Shen, Z. X. *Nano Lett.* **2015**, 15, 8155-8161